KTH Industrial Engineering
and Management

On high temperature oxidation resistance

Towards the materials genome of high temperature alloys

SAMUEL HALLSTRÖM

Doctoral Thesis
Stockholm, Sweden 2014

Materialvetenskap
KTH
SE-100 44 Stockholm

ISBN 978-91-7595-313-7

Akademisk avhandling som med tillstånd av Kungl Tekniska högskolan framläges till offentlig granskning för avläggande av doktorsexamen fredagen den 14:e november 2014 kl 10:00 i sal B2, Brinellvägen 23, Kungliga Tekniska Högskolan, Stockholm. Fakultetsopponent är Professor Roger Reed, University of Oxford, England.

© Samuel Hallström, November 2014

Tryck: Universitetsservice US AB

Abstract

The efficiency of a heat engine increases with increasing service temperature. This leads to a demand for material that can withstand aggressive environments and sometimes also high load at higher and higher temperature. That is the rationale for the work of this thesis. It is divided into two parts, both addressing model alloy systems for components used in oxidizing high temperature environments.

In the first part the phase equilibria and phase diagrams of Ni-Ru and Al-Ni-Ru are investigated from a thermodynamic point of view using the well known Calphad method. In particular, the debated existance of a miscibility gap between the aluminides NiAl and RuAl is considered. This led to a combined ab initio/Calphad approach and it is suggested that there is a miscibility gap at low temperature.

In the second part, first of its kind diffusion simulations in oxides are performed in the technologically important Fe-O and Cr-O systems. In the simulations, the moving phase boundary problem is solved with use of temperature and composition dependent diffusion coefficients, that are evaluated for complex oxide phases modeled with up to four sublattices. This type of simulations attracts a lot of interest and it looks very promising for future extension to higher order systems.

Keywords: Diffusion, Thermodynamics, Simulation, Multicomponent, Kinetics, Phase transformations, Calphad.

To my unborn child

Acknowledgement

It took a bit longer than expected to complete this thesis, hence I am grateful to many people.

Professor John Ågren, my supervisor. First for being an excellent teacher, making me interested in phycial metallurgy during my years as an undergraduate. Then also for giving me the opportunity to do this work, for his guidance and for interesting discussions. Also, I would like to thank him for his never-ending patience.

My co-authors and all former colleagues at the Department of Materials Science and Engineering, for a good working atmosphere. Special thanks go to Dr. Johan Jeppsson, Dr. Lars Höglund, Dr. Torbjörn Jonsson, Profs. Malin Selleby, Annika Borgenstam, and to Mr. Thomas Barkar, Dr. Lina Kjellqvist, and Prof. Bo Sundman.

All my current colleagues at Thermo-Calc Software, for making it so fun to be at work.

Thermo-Calc Software, for support and encourgement to finish this work.

My friends.

My family, for always believing in me and for always being there.

Josefin and Noah, for being two of the most important persons in my life, and for the love and support during the final work of this thesis.

For the financial part I would like to thank the following:

Stiftelsen Jernkontorsfonden för Bergsvetenskaplig Forskning, for making a leave of abscence from Thermo-Calc possible, during which I could finalize this thesis.

Papers I and II are part of the Hipercoat project, financed by the European Commission (GRD2-200-30211), and the National Science Foundation (DMR-0099695).

Papers III-V were sponsored by the Swedish Foundation for Strategic Research within the CROX and CCT programs.

List of publications

The research presented in this thesis was performed at the Division of Physical Metallurgy, Department of Materials Science and Engineering, School of Industrial Engineering and Management, KTH (Royal Institute of Technology), Stockholm, Sweden. The thesis consists of an introduction to this field and the following attached papers:

I Thermodynamic Assessment of the Ni-Ru system
Samuel Hallström, Journal of Phase Equilibria and Diffusion, Volume 25, Number 3, (2004), 252-254

II Thermodynamic reassessment of the Ni-Ru system and assessment of the Al-Ni-Ru system at 1273-1523 K using ab initio calculations
Samuel Hallström, David Andersson, Andrei Ruban, John Ågren, Acta Materialia, Volume 56, Issue 15, (2008), 4062-4069

III Modeling of diffusion in wustite and simulation of oxidation of iron at 600°
Samuel Hallström, Lars Höglund, John Ågren, The 6th European Stainless Steel Conference, Science and Market, Helsinki, Finland, June 10-13, (2008)

IV Modeling of iron diffusion in the iron oxides magnetite and hematite with variable stoichiometry
Samuel Hallström, Lars Höglund, John Ågren, Acta Materialia, Volume 59, Issue 1, (2008), 53-60

V High temperature oxidation of chromium: kinetic modeling and microstructural investigation
Samuel Hallström, Mats Halvarsson, Lars Höglund, Torbjörn Jonsson, John Ågren, Solid State Ionics, Volume 240, (2013), 41-50

Contents

Chapter 1

Introduction

The scientific field of computational thermodynamics aims at predicting a material's properties by computations, rather than measuring them experimentally. The rationale for doing so is manifold. Experimental work is often both expensive and tedious, and there is often a lot to gain if the number of experiments can be reduced. If physically sound models are used, computer simulations can not only help to understand phenomena, but also predict ones that are not known.

For high temperature applications, which the present work addresses, the materials often possess special characteristics compared with material used at ambient temperature. Oxidation, creep, and sometimes even evaporation play important roles at elevated temperatures. In oxidation, one or more components react with oxygen to form one or more oxides. Often, this is an unwanted process in which the material's mechanical properties deteriorate as a consequence of losing important alloying elements by oxidation and perhaps evaporation. Often high-temperature applications involve high loads and the materials need to have good creep resistance.

1.1 Gas turbine engines and thermal barrier coatings

A gas turbine is an axial combustion engine used predominantely for propulsion of aircraft or generation of electrical power. The general principles of a gas turbine engine are remarkably simple. Air is compressed, mixed with fuel and ignited. The expanding hot gases drive turbines which in turn continue to compress air. Depending on the type of engine, the hot expanding gases either produce thrust or drive a power generator. In addition to high mechanical load, material in the hot parts of a gas turbine engine can be exposed to aggressive oxidizing environments and temperature differences in excess of 1200 °C, e.g. [1, 2]. The reason for using such high temperature is, that the higher the temperature, the more efficient is the engine. Designed for this purpose is a class of material called superalloys.

Thus superalloys have superior high temperature capacities compared with other metallic alloys. They are based on nickel, cobalt, or nickel-iron. In this work, the nickel-based superalloy type is considered. The microstructure of a nickel-based superalloy usually consists of coherent cubic particles of gamma-prime ($\gamma\prime$), which is an ordered fcc phase based on the nominal description Ni_3Al, in a continuous matrix of disordered fcc, called gamma (γ). The main strengthening of a precipitate hardened nickel-base alloy comes from $\gamma\prime$, but solution hardening from alloying elements in γ is also present.

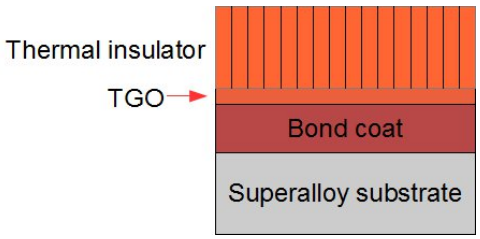

Figure 1.1: A schematic image showing the different layers of a thermal barrier coating.

The extreme service conditions and the required component lifetime of today can not be matched by a single material. Internal channels in the turbine blades for cooling air decrease the temperature at the alloy surface. Through several generations of superalloys and advanced coating techniques, the materials that are used in the hot load-bearing parts consist of complex multi-layered structures, where the chemistry and dimensions are carefully engineered. They go by the name *thermal barrier coating* (TBC), the structure is schematically shown in fig.1.1. The different layers all have their purpose. The actual thermal barrier usually consists of a deposited columnar layer of 7 weight percent yttria stabilized zirconia (7-YSZ) [1], approximately 100-250 μm thick [2], giving a temperature drop of about 200 °C [3]. In stationary components it can be thicker, up to about 1 mm [2]. Oxidation protection is achieved by the thermally grown oxide (TGO), which is always alumina (Al_2O_3), and the bond coat [2]. Without controlled oxidation, the alloy substrate would loose aluminum, which would lower the amount of strengthening $\gamma\prime$ and consequently also lower service lifetime. By allowing alumina to grow, the oxidation rate can be controlled and predicted. The bond coat is rich in aluminum, and serves as a reservoir of aluminum for the TGO. Common types of bond coat are a single configurationally ordered bcc phase (β) based on nickel-aluminide, and a two-phase γ/β structured MCrAlY type coating. The thickening rate of the TGO is one important factor determining the lifetime of a component. Its growth rate is primarily determined by inward diffusion of oxygen, but outward diffusion of aluminum cannot be neglected. Also the bond coat should act as a diffusion barrier for alloying elements, which favors the ordered β.

1.2 9-12 % chromium steel for high temperature applications

Creep and oxidation resistant chromium steel is used e.g. in turbines, boilers and steam lines in steam power plant for generation of electrical power, operated at temperatures up to about 600 °C [4]. At such high temperature and in the aggressive environment of e.g. biomass-fueled power plants, high alloyed stainless steel with > 9 % Cr is used. One such family of material is the 9-12 % chromium steel. The microstructure consists of a matrix of tempered martensite and precipitated particles, giving particle hardening effect which increases the creep strength. The precipitates also retard the coarsening of the martensite structure. Two favorable precipitate phases are the $M_{23}C_6$ carbide and the MX carbonitride. In $M_{23}C_6$, M is mainly Cr, Fe, W and Mo. In MX, M is V or Nb, X is C or N. Often the steel contains tungsten as a solid-solution strengthener, but formation of the Laves phase (mainly Fe_2W) reduces the creep resistance.

The oxidation resistance relies on the protective oxide $(Cr_xFe_{1-x})_2O_3$. In presence of water vapour, Cr is lost to the environment by evaporation of $CrO_2(OH)_2$[5]. If the evaporation rate becomes too high, the oxide can loose its protective behaviour by forming less favourable oxides, e.g. Fe_2O_3 and $FeCr_2O_4$.

1.3 Overview of this work

In this thesis, different aspects of material used in two kinds of high temperature applications are addressed. They have in common that they both address model alloy systems for components used in oxidizing high temperature environments, and that the Calphad technique has been the basis for the tools used in this work. First, thermodynamic assessments have been made for the Ni-Ru and Al-Ni-Ru systems, which are alloy systems related to nickel-based superalloys used in the hot parts of gas turbine engines.

Second, oxidation and diffusion in oxides are addressed in a general way based on the classical theories of Wagner. This work is the first of its kind, but uses much knowledge from similar treatment of other types of material. The full diffusion problem is solved numerically for oxidation of iron and chromium.

For the thermodynamic part of this work, the software Thermo-Calc [6] was used. For kinetic modeling and diffusion simulations, the software DICTRA [6] was used. For model development, the application programming interface TC-Toolbox for MATLAB® [7] was extensively used.

Chapter 2

The materials genome

In 2011, US President Barack Obama announced an initiative similar to the systematic mapping of the human genome, but with the goal of building an infrastructure meant to significantly reduce the time it takes new materials to reach the market [8]. That infrastructure will include "... leveraged computational capabilities, data management, and an integrated approach to materials science and engineering". To achieve the goals laid out in the initiative, a few steps are listed. They include developing software for design of materials, characterization tools that should aid model and software development, and development of standards and databases. Together with their definition of a materials genome[1], it is interesting to note that it sounds very familiar if you are introduced to the Calphad method (see section 3.1). As shown by Kaufman and Ågren [9], Calphad, as a method or framework, has all the parts of a materials genome because the method is about storing only the essential data required for calculation of a material's equilibrium state or dynamic properties. An equilibrium state or the dynamic properties of a material can be computed if the thermodynamic and kinetic properties of all the phases of the system are known. Thus one problem to solve is to store only the essential data and nothing else. The Calphad method approaches this in a powerful way. The method is often referred to as semi-empirical. It is fundamental in the sense that physical models are used, which follow the fundamental laws of thermodynamics. It is empirical in the sense that results from experiments are of tremendous importance. It is worth noting that the word 'experiments' in this case does not necessarily have to refer to actual experimental data. In situations when real experiments are hard or impossible to perform, they can be complemented by using other information, for example calculations using methods like DFT (density functional theory), simple rules of thumb or anything in between. This way, Calphad

[1] Materials genome definition [8]: "A genome is a set of information encoded in the language of DNA that serves as a blueprint for an organism's growth and development. The word genome, when applied in non-biological contexts, connotes a fundamental building block toward a larger purpose."

makes it possible to use all collected knowledge about thermodynamics and kinetics and use it for solving real practical problems. The individual experiments themselves are not stored in databases. Instead, experiments of any kind that can be calculated from thermodynamics are used in an 'assessment' procedure, in which model parameters are adjusted until they, when used in computations, reproduce all the considered experimental data. When the model parameters of all phases of a system have been determined, it is possible to compute thermodynamic or dynamic properties or functions thereof that perhaps never have been measured. The predictive capabilities using this approach are excellent, provided that the models are advanced enough to be able to resolve the properties of interest, and also that the experimental data is of good quality. Often though, there is a trade-off between computation time and capability of the model. Selecting a too simple model for a phase might later require it to be replaced with a more advanced one. This, and the fact that sometimes there is a need to reassess a system, are one of the great challenges of Calphad today. Currently it requires a great effort to do such changes to an existing large database, a situation that could preferably be made much more automatic. Another great challenge related to the materials genome initiative that also involves Calphad, is a desire to direct couple thermodynamic properties to mechanical and other properties on different length scales. This is usually referred to as Integrated Computational Materials Engineering (ICME).

Today there are powerful software products available that successfully handle many real industrial problems. This work contributes to the never-ending need to extend the thermodynamic and kinetic databases and to develop new models that can be used in the materials design process.

Chapter 3

Thermodynamic modeling

3.1 Calphad

Since the late sixties, starting with the initiatives and pioneering work of Larry Kaufman, Himo Ansara and Mats Hillert, a new scientific field called computational thermodynamics has developed [10]. They founded a community and collection of working methods called Calphad, a portmanteau for "calculations of phase diagrams". A phase diagram is a useful graphical representation of an alloy's equilibrium states, but today the Calphad community does more than that. The community consists of scientists from all around the world, working with software, model and database development to improve not only the accuracy and complexity, but also the types of materials considered in the computations.

3.2 Computational thermodynamics

In computational thermodynamics, phase diagrams and thermodynamic properties are computed based on the basic thermodynamic properties of the system. The basic thermodynamic properties are represented by consistent mathematical expressions, usually of the Gibbs energy as functions of temperature and composition, for phases in the considered system. These expressions should be kept as simple as possible, but be physically sound. The process of obtaining a consistent set of thermodynamic data for a system is called a thermodynamic assessment. An assessment procedure usually begins with a literature study, in which all available thermochemical and phase diagram data is obtained. If necessary and if possible, additional key experiments can be performed. Suitable thermodynamic models for the different phases should be selected and after that the actual procedure begins, where model parameters are adjusted to fit the experimental data. That last step is usually aided by some minimization software. The next few sections describe the thermodynamic models which have been used in the present work.

3.2.1 Ideal solution

When different species are mixed and all the intermolecular forces can be neglected, or if they on the average are the same, the solution is said to be ideal. If all species mix ideally, the change in Gibbs energy upon mixing the pure species comes only from the increase in entropy:

$$\Delta^{ideal}G_m = -T\Delta S = -RT\sum x_i ln(x_i) \tag{3.1}$$

The species of an ideal solution always mix spontaneously. Often, it is a good approximation to model gases as ideal, and that is a common practice in Calphad.

3.2.2 The regular solution model

If a solution deviates from ideality, it means that there is some interaction between the mixed species. The interaction can either be attractive or repulsive, and this will result in a non-zero enthalpy of mixing. In Calphad, it is common to model disordered solution phases with the regular solution model. The Gibbs energy for a phase is written:

$$\Delta G_m = \Delta H - T\Delta S = {}^0G_m + \Delta^{ideal}G_m + {}^EG_m \tag{3.2}$$

where

$${}^0G_m = \sum x_i {}^0G_i \tag{3.3}$$

is the Gibbs energy coming from the pure species. x_i and ${}^0G_i$ are the molar fraction and Gibbs enery of the pure species i, respectively. The term ${}^EG_m$ is called the excess Gibbs energy and it contains the deviation from ideal behaviour. Usually in Calphad the excess Gibbs energy is described with Redlich-Kister polynomials:

$${}^EG_m = \sum_i \sum_{j<i} x_i x_j \left(\sum_{r=0}^{m} {}^r\Phi^{i,j}(x_i - x_j)^r \right) \tag{3.4}$$

where ${}^r\Phi^{i,j}$ are parameters describing the interaction between species. During the assessment these interaction parameters are optimized to fit the experimental data and stored in thermodynamic databases.

3.2.3 The compound energy formalism

For solution phases showing chemical ordering, or other solution phases with more complex crystallographic structure represented by more than one sublattice, it is common to use the compound energy formalism, which is described in detail in [11]. The phase is described using a simple sublattice notation. For example, if the species A and B mix on sublattice s, and D and E on sublattice t, it is described as $(A,B)_k(D,E)_l$. $n^s = k$ and $n^t = l$, stoichiometric factors, denote the number of sites on each sublattice. If A, B, C and D are simple atoms, one formula unit thus contains $k + l$ atoms. The composition on a sublattice and in the phase as a whole can change. In addition to the regular mole fraction of i, x_i, it is convenient to introduce the fraction of i on sublattice s, y_i^s, the so-called site fraction. The condition $\sum_i y_i^s = 1$ must be fulfilled if the fraction of vacant lattice sites are included in the summation.

A combination of one species on each sublattice, i.e. the real or hypothetical compound of the type A_kD_l is called an end-member.

The Gibbs free energy of a phase is expressed as:

$$\Delta G_m = G_m^{s.r.} - TS_m^{mix} + {}^E G_m \tag{3.5}$$

where

$$G_m^{s.r.} = \sum {}^0 G_{end} \Pi y_i^s \tag{3.6}$$

is a weighted average of the end-members' Gibbs energies. *s.r.* stands for surface of reference. Πy_i^s is the product of all the end-member's site-fractions. ${}^0G_{end}$ is given relative some standard state of the end-member's components.

The entropy contribution to the Gibbs energy is obtained assuming random mixing within each sublattice, and is expressed as

$$S_m^{mix} = -R \sum_s \sum_i n^s y_i^s ln(y_i^s) \tag{3.7}$$

The last term of equation 3.5 is the excess Gibbs energy

$${}^E G_m = \Pi y_i^s \sum y_B^t L_I \tag{3.8}$$

where I denotes an arbitrary combination of species on different sublattices.

The interaction parameters L usually take the form of a Redlich-Kister polynomial in the binary case

$$L_{ij} = \sum_v (y_i - y_j)^v \times {}^vL_{ij} \tag{3.9}$$

In the ternary case, the interaction parameter is expressed as

$$L_{ijk} = v_i{}^iL_{ijk} + v_j{}^jL_{ijk} + v_k{}^kL_{ijk} \tag{3.10}$$

where

$$v_i = y_i + (1 - y_i - y_j - y_k)/3 \tag{3.11}$$
$$v_j = y_j + (1 - y_i - y_j - y_k)/3 \tag{3.12}$$
$$v_k = y_k + (1 - y_i - y_j - y_k)/3 \tag{3.13}$$

For a phase with order/disorder transitions, it is possible to describe the Gibbs energy with one single mathematical function. Such a case is described with a contribution to the Gibbs energy from chemical ordering:

$$G_m = G_m^{dis}(x_i) + \Delta G_m^{ord}(y_i^s) \tag{3.14}$$

If the phase is disordered, that contribution must be zero, and that can be ensured by postulating the following expression:

$$\Delta G_m^{ord} = G_m^{ord}(y_i^s) - G_m^{ord}(y_i^s = x_i) \tag{3.15}$$

where G_m^{ord} is given by 3.5.

Chapter 4

Kinetic modeling

4.1 Diffusion in chemical potential gradients

Depending on the context, the word diffusion can have many different meanings. Throughout this thesis, the meaning of diffusion will be that of transport of atoms or ions in solid state. In that context, diffusion is very often explained in relation to a famous equation called the Fick's first law of diffusion, which relates the amount of atoms that diffuses to a difference in concentration:

$$J_k = -\tilde{D}\frac{\partial c_k}{\partial z} \tag{4.1}$$

J_k is the flux of k, i.e. the amount of k per unit time and unit area. The factor of proportionality $\tilde{D}_k$ is the chemical diffusion coefficient of k, c_k is the concentration of k expressed as amount per unit volume, and z is a spatial variable in one dimension. The minus sign makes the flux positive when diffusing from regions with high concentration to regions with low concentration. From a thermodynamic point of view however, the driving force for diffusion is the gradient in chemical potential. Eq. 4.1 can be brought to that form:

$$J_k = -\tilde{D}\frac{\partial c_k}{\partial z} = -L_k\frac{\partial \mu_k}{\partial z} = -L_k\frac{\partial \mu_k}{\partial c_k}\frac{\partial c_k}{\partial z} \tag{4.2}$$

It can be noted that this form is analogous to Ohm's and Fourier's laws for charge and heat transfer.

Since mass is a conserved quantity, its transport can be described with a continuity equation:

$$\frac{\partial c_k}{\partial t} = \frac{\partial}{\partial z}(-J_k) \tag{4.3}$$

For simple cases, the continuity equation can be solved analytically, however for most practical problems numerical solutions are the only reasonable choices.

The diffusion coefficient in eq. 4.1 is called chemical diffusion coefficient or inter-diffusion coefficient. It can be evaluated if a point in the material can be defined, where the total amount of atoms on each side remains constant during the diffusion process. From such a position it appears as if the atoms in a binary system just exchange place with each other and diffusion occurs in the number-fixed frame of reference. The concept of frames of reference is important, since depending on the chosen frame of reference, different types of information is available. If instead a frame of reference is selected, such that it is fixed relative to the crystal lattice, it is called the lattice-fixed frame of reference. In that frame of reference, it is possible to determine the tracer diffusion coefficients (denoted D_k^*), and the individual diffusion coefficients (denoted D_k).

Eq. 4.1 is valid in ideal binary systems. A more general approach was later made by Onsager, who formulated an equation for multi-component systems with all the different thermodynamic driving forces for diffusion (e.g. gradients in chemical potential, electric potential, temperature):

$$J_k = -\sum(L_{kj}X_j) \tag{4.4}$$

The L factors are phenomenological kinetic parameters, and the X factors are the driving forces. The most common case would be a system with constant pressure and temperature. Eq. 4.4 then becomes:

$$J_k = -\sum_{j=1}^{N}(L_{kj}\frac{\partial \mu_j}{\partial z}) \tag{4.5}$$

where N is the number of components and the derivative $\partial\mu_j/\partial z$ is the gradient in chemical potential of j. For practical purposes it is often more convenient to express the flux as function of concentration gradient instead of gradient in chemical potential. Using the chain-rule of differentiation, and the assumption that $\mu_j = \mu_j(c_1, c_2...c_N)$ eq. 4.5 becomes:

$$J_k = -\sum_{j=1}^{N}(L_{kj}\sum_{i=1}^{N}\frac{\partial \mu_j}{\partial c_i}\frac{\partial c_i}{\partial z}) \tag{4.6}$$

This expression describes how the flux of a component depends on all concentration gradients. The proportionality factor matrix D_{ki} can be expressed as:

$$\tilde{D}_{ki} = \sum_{j=1}^{N} L_{kj}\frac{\partial \mu_j}{\partial c_i} \tag{4.7}$$

The concentrations are not independent and it is convenient to eliminate one of them, say N, and eq. 4.7 becomes:

$$\tilde{D}^N_{ki} = \sum_{j=1}^{N-1} L_{kj}(\frac{\partial \mu_j}{\partial c_i} - \frac{\partial \mu_j}{\partial c_N}) \tag{4.8}$$

$\tilde{D}^N_{ki}$ is usually called the reduced diffusion coefficient matrix. eq. 4.6 becomes:

$$J_k = -\sum_{i=1}^{N-1}\tilde{D}^N_{ki}\frac{\partial c_i}{\partial z} \tag{4.9}$$

Insertion of eq. 4.9 in eq. 4.3 gives a diffusion equation for multi-component cases:

$$\frac{\partial c_k}{\partial t} = \frac{\partial}{\partial z}(\sum_{i=1}^{N-1}\tilde{D}_{ki}\frac{\partial c_i}{\partial z}) \tag{4.10}$$

4.2 Implementation - the DICTRA software

The following section describes the background of one implementation of the diffusion theory: the DICTRA [6] software. DICTRA is a portmanteu of "diffusion controlled transformations" and it allows the diffusion equation to be solved numerically in one dimension for quite complex problems.

In order to solve eq. 4.9, the diffusion coefficient matrix in eq. 4.8 is needed. As can be seen, it consists of two parts: the L parameters that are purely kinetic, and

the derivatives of the chemical potentials, which are purely thermodynamic. If the thermodynamic properties of the phases of interest in the system are known - for example as described in section 3.1 - the thermodynamic part can be calculated. One successful approach to treat modeling of the kinetic parameter was suggested by Andersson and Ågren[12]. Instead of the diffusion coefficient, they found that it is superior to store the atomic mobility. One great advantage with that is that instead of the $(N-1)(N-1)$ number of diffusion coefficients one would have to store in a database, there were only N mobilities. By taking the thermodynamic part from the already known thermodynamic descriptions, one would automatically use much prior knowledge about the system.

For crystalline phases, the predominant diffusion mechanism is an atom or ion exchanging place with a neighboring vacancy. With absolute reaction-rate arguments, and with the assumption that the amount of vacancies is in equilibrium, Andersson and Ågren[12] expressed the flux of substitutional k in the lattice-fixed frame of reference as:

$$\tilde{J}_k = -c_k y_{Va} \Omega_{kVa} \frac{\partial \mu_k}{\partial z} \tag{4.11}$$

where Ω_{kVa} is the rate of exchange between a vacancy and a neighboring k atom. Ω_{kVa} is related to the atomic mobility M_k:

$$M_k = y_{Va} \Omega_{kVa} \tag{4.12}$$

eq. 4.11 becomes:

$$\tilde{J}_k = -c_k M_k \frac{\partial \mu_k}{\partial z} \tag{4.13}$$

Using absolute reaction-rate arguments, the mobility can be described with an Arrhenius expression:

$$M_k = \frac{M_k^0}{RT} \exp(\frac{-Q_k}{RT}) \tag{4.14}$$

M_k^0 is the frequency factor and Q_k is the activation energy. The factor of proportionality $c_k M_k$ can be identified as the factor L_{kk} that relates flux to driving force.

In general, both Q_k and M_k^0 depend on composition. In a similar manner as thermodynamic modeling using the Calphad method, the composition dependence is expressed as a linear combination of the end-point values and a Redlich-Kister expansion:

$$\Phi = \sum_i x_i \Phi^i + \sum_i \sum_{j<i} x_i x_j \left(\sum_{r=0}^{m} {}^r\Phi^{i,j} (x_i - x_j)^r \right) \tag{4.15}$$

where Φ represents either M_k or $-Q_k$.

4.3 Diffusion models in DICTRA

There are several diffusion models available in the DICTRA software [6]. The most common one is the default model described above, that computes the full diffusion coefficient matrix for phases. It has a constraint on the phase description: no phase constituents other than elements are allowed, and the site-fractions should be possible to determine from the u-fractions[1]. This is sufficient for many technically important diffusion controlled problems, including moving phase boundary problems with phases like austenite and ferrite.

Ordering effects in phases with chemical ordering, see section 3.2.3, can be taken into account using the ordered model. Using that model, there is a contribution to the mobility's activation energy from the degree of chemical ordering[13]. In such cases there is a significant increase in the activation energy as the phase becomes more and more ordered. This model is suitable for intermetallic phases like NiAl with B2 ordering.

Some phases have diffusion mechanisms that cannot be successfully modelled with the default or ordered models in DICTRA. Oxides is one example and of those, one particularly pedagogical example is magnetite, Fe_3O_4, which has a considerable stable range of composition and shows a minimum in cation tracer diffusion coefficient close to the stoichiometric composition. That behavior can not be generically modeled with a single atomic mobility. The phase is modeled with the same species on several sublattices and the site occupancy is dependent not only on temperature but also on the overall composition.

For such complex phases, there is now a so-called "general diffusion model" available. It takes as input individual mobilities for all species on all sublattices. From those

[1] The u-fraction is a composition variable that comes from an assumption that only substitutional atoms contribute to volume. It is defined as $u_k = x_k(\sum_{j \in S} x_j)^{-1}$ where x is the regular mole-fraction and S is all substitutional atoms.

mobilities an effective mobility for each element is calculated and that effective mobility enters the diffusion equation. The general diffusion model will be described in more detail for oxides in the following sections.

4.4 Diffusion in oxides

The following treatment of diffusion in oxides is based on the important work of Wagner on transport in oxides, e.g. [14, 15]. Formulating the basic principles behind defect chemistry and oxidation kinetics, Wagner realized the importance of the vacancy for diffusion of atoms and ions. He derived expressions for e.g. defect concentrations and fluxes using the Kröger-Vink notation, while in this work the sublattice formalism is applied.

In this work some binary oxides are considered. The O^{-2} ion is considerably larger than the metal cations, see for example ref. [16], and may be regarded as building up the lattice having cations in the interstices. These oxides thus have in common that their thermodynamic models contain one sublattice that solely contains oxygen anions. The other (interstitial) sublattces can contain cations and vacancies. Using the sublattice notation (see the beginning of section 3.2.3), such a phase can be described as:

$$(C_1, C_2 ... C_{N_1})_{a^1} (C_1, C_2 ... C_{N_2 - 1}, Va)_{a^2} (O^{-2})_{a^O} \tag{4.16}$$

Va denotes vacancies and the species C_i are cations in this case. There can be no or several sublattices of the first type (without vacancies), and there can be one or more sublattices of the second type (with vacancies). The same species may or may not occur on more than one sublattice. For all calculations it was assumed that cation diffusion occurs only on sublattices that contain vacancies because the vacancy mechanism is operative.

If we in eq. 4.4 also take into account a gradient in electic potential, the flux of k would become:

$$J_k = -L_k(\frac{\partial \mu_k}{\partial z} + \alpha_k F \frac{\partial \phi}{\partial z}) \tag{4.17}$$

where ϕ is electric potential, α_k the charge of k (e.g. -1 for the electron and -2 for the oxygen ion) and F is the Faraday constant.

Consider a case where there is no external electric potential applied to the system, only a gradient in chemical potential e.g. from an oxidizing atmosphere. Electric

charge is not expected to build up in the specimen subjected to the gradient in chemical potential. Then there is no net flow of charge, thus the sum of fluxes of all charges must equal zero. For the phase in eq. 4.16, that condition becomes:

$$\sum_{s\in S}\sum_{n}\alpha_{C_n}J_{C_n} - 2J_{O^{-2}} - J_{e^{-1}} = 0 \tag{4.18}$$

S is all interstitial sublattices that contain vacancies. The expressions for the fluxes in the charge balance equation become:

$$J_{C_n} = -L_{C_n}(\frac{\partial\mu_{C_n}}{\partial z} + \alpha_{C_n}F\frac{\partial\phi}{\partial z}) \tag{4.19}$$

$$J_{O^{-2}} = -L_{O^{-2}}(\frac{\partial\mu_{O^{-2}}}{\partial z} - 2F\frac{\partial\phi}{\partial z}) \tag{4.20}$$

$$J_e = L_eF\frac{\partial\phi}{\partial z} \tag{4.21}$$

Following the analysis of Peterson and Chen [19], we assume that for the present cases the elctrons are much more mobile than the ions. This means that the electron flux necessary for keeping the charge balance equation fulfilled is not limiting the movement of ions. This also implies that it is not not necessary to distinguish between different valences when solving the diffusion equation.

With the above assumptions, using absolut reaction-rate arguments, the flux of an interstitial element k in the lattice-fixed frame of reference is postulated:

$$J_k = -\frac{1}{a^O V_m}\sum_{s\in S}(a^s\, y^s_{Va}\sum_{n\in K} y^s_{C_n}M^s_{C_n})\frac{\partial\mu_k}{\partial z} \tag{4.22}$$

K is all species on sublattice s that contain k. V_m is the volume per mole of anion sites. a^O is the stoichiometry factor (number of sites per formula unit) of the substitutional anion sublattice, and a^s is the stoichiometry factor for the interstitial sublattice s. $y^s_{C_n}$ is the site-fraction of C_n on sublattice s, and $M^s_{C_n}$ is the mobility of C_n on sublattice s.

Often, tracer diffusion coefficients are reported in the literature. From eq. 4.22 it is useful to derive the expression for the tracer diffusion coefficient D_{k^*}. From a small amount of the tracer k^* added to a homogeneous system, redistribution of the tracer can be observed and obeys the following flux equation:

$$J_{k^*} = -\frac{1}{a^O V_m} \sum_{s \in S} (a^s y^s_{Va} \sum_{n \in K} y^s_{C^*_n} M^s_{C_n}) \frac{\partial \mu_{k^*}}{\partial z} \tag{4.23}$$

Where C^*_n is a tracer cation.

The tracer distributes randomly between the different sublattices, and from that it can be concluded that the ratio between the tracer and non-tracer species is the same in all sublattices and in the system, giving:

$$\frac{y_{C^*_n}}{y_{C_n}} = \frac{n_{k^*}}{n_k} \tag{4.24}$$

Where n_{k^*} and n_k are the total number of tracers and non-tracers per anion site. Inserting $y_{C^*_n} = y_{C_n} \frac{n_{k^*}}{n_k}$ and $\mu_{k^*} = RTln\frac{n_{k^*}}{n_k}$ in eq. 4.23 gives:

$$J_{k^*} = -\frac{1}{a^O V_m} \sum_{s \in S} (a^s, y^s_{Va} \sum_{n \in K} y^s_{C_n} M^s_{C_n}) \frac{n_{k^*}}{n_k} \frac{\partial RTln\frac{n_{k^*}}{n_k}}{\partial z} \tag{4.25}$$

Taking the derivative and using the chain rule to replace the gradient in chemical potential with concentration gradient, and the relation $c_{k^*} = n_{k^*}/V_m$, gives:

$$J_{k^*} = -\frac{1}{a^O V_m} \sum_{s \in S} (a^s y^s_{Va} \sum_{n \in K} y^s_{C_n} M^s_{C_n}) \frac{n_{k^*}}{n_k} RT \frac{\partial ln\frac{n_{k^*}}{n_k}}{\partial \frac{n_{k^*}}{V_m}} \frac{\partial c_{k^*}}{\partial z} \tag{4.26}$$

$$J_{k^*} = -\frac{RT}{a^O n_k} \sum_{s \in S} (a^s y^s_{Va} \sum_{n \in K} y^s_{C_n} M^s_{C_n}) \frac{\partial c_{k^*}}{\partial z} \tag{4.27}$$

The tracer diffusion coefficient is identified as:

$$D_{k^*} = \frac{RT}{a^O n_k} \sum_{s \in S} (a^s y^s_{Va} \sum_{n \in K} y^s_{C_n} M^s_{C_n}) \tag{4.28}$$

Eq. 4.22 can now be expressed in terms of the tracer diffusion coefficient:

$$J_k = -\frac{D_{k^*}}{RT} \frac{n_k}{V_m} \frac{\partial \mu_k}{\partial z} \tag{4.29}$$

From eq. 4.2 and $c_k = n_k/V_m$ we can obtain the chemical diffusion coefficient from 4.29:

$$D_k = L_k \frac{\partial \mu_k}{\partial c_k} = \frac{D_{k^*} n_k}{RT\, V_m} \frac{\partial \mu_k}{\partial \frac{n_k}{V_m}} = \frac{D_{k^*} n_k}{RT} \frac{\partial \mu_k}{\partial n_k} \tag{4.30}$$

On the anion sublattice usually there are no vacancies in the thermodynamic model, assuming a low amount of thermal vacancies only. The oxygen diffusion is treated in a simpler and similar way as substitutional atoms in eq. 4.12.

If the thermodynamic description is known, all variables except the mobilities can be calculated. The mobilities take the form of eq. 4.14. The values of the pre-exponential factors and activation energies are unknown, but can be obtained by optimizing against experimental data.

4.5 Approximate treatment of grain boundary diffusion

The dominating migration path of a diffusing species can vary significantly depending on temperature. Diffusion is generally faster the more disordered the surrounding is for a diffusing species. All materials contain structural elements that provide fast diffusion paths, but their effect on the overall behavior varies greatly with process and service condition. Examples of such fast diffusion paths are grain boundaries, dislocations and surfaces.

At the service temperature of the chromium steel considered in this work, the oxidation rate is highly dependent on grain boundary diffusion. The grain boundary diffusion has been taken into account by computing effective mobilities from the mobilities assuming so-called type A kinetics [20].

$$M_{eff} = f_{gb} M_{gb} + (1 - f_{gb}) M_b \tag{4.31}$$

Where $f_{gb} = \delta/\phi$ is an approximation of an assigned volume fraction of grain boundaries. $\delta \approx 5$Å is the approximate grain boundary width and ϕ is the oxide grain size. This approximation is valid for conditions when the diffusion front is essentially planar, e.g. for long diffusion times and grains small enough, so that the diffusion fields around neighboring grain boundaries overlap.

The grain boundary diffusional mobility, M_{gb}, is assumed to be of Arrhenius type and with the same pre-exponential factor as for bulk diffusion. Rule-of-thumb values have been used for the activation energy $Q_{gb} = \alpha Q_b$, where $\alpha < 1$.

4.6 Growth of external oxide layers

When a material oxidizes, usually at least three phases are present. The oxidizing metal, the oxide, and the surrounding atmosphere that contains oxygen. This is schematically shown in fig. 4.6, which has two interfaces, oxide/gas and oxide/metal.

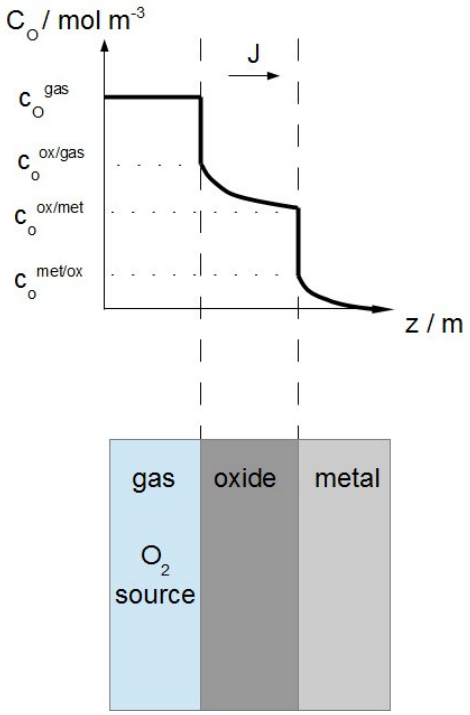

Figure 4.1: Schematic figure showing the concentration profile for oxide layer formation.

It is assumed that the phase interfaces are perfectly mobile and that diffusion across the interfaces occurs without dissipation of driving force. For each of these interfaces it is possible to set up flux balance equations from which it is possible to determine the total oxidation rate. By considering conservation of the amount of diffusing species across a moving phase boundary for some small amount of time, the following general flux balance equations can be derived for each phase interface between the phases α and β in a binary A-O system:

$$\frac{v^{\beta/\alpha}u_A^{\beta/\alpha}}{V_s^\beta} - \frac{v^{\alpha/\beta}u_A^{\alpha/\beta}}{V_s^\alpha} = J_A^\beta - J_A^\alpha \tag{4.32}$$

$$\frac{v^{\beta/\alpha}u_O^{\beta/\alpha}}{V_s^\beta} - \frac{v^{\alpha/\beta}u_O^{\alpha/\beta}}{V_s^\alpha} = J_O^\beta - J_O^\alpha \tag{4.33}$$

$v^{\alpha/\beta}$ and $v^{\beta/\alpha}$ are the velocities of the phase interface on the respective side. The relation $c_k = u_k/V_s$ was used, where V_s is the molar volume per substitutional atom in a phase. The direction of a moving phase boundary can often be estimated by some rather simple reflections. If the above equations are applied to the oxide/metal interface, we can identify β as the oxide and α as the metal. In the metal, oxygen atoms dissolve interstitially between substitutional metal atoms, while the opposite is true for oxides. Consequently $u_O^{ox/met} = 1$ and $u_A^{met/ox} = 1$. Since the oxygen content in the metal is very low, the following reasonable assumptions can be made: $u_O^{met/ox} \approx 0$, $u_A^{met/ox} \approx 1$, $J_O^{met} \approx 0$, $J_A^{met} \approx 0$. The flux balance equations for such a case are reduced to:

$$\frac{v^{ox/met}}{V_s^{ox}} = J_O^{ox} \tag{4.34}$$

$$\frac{v^{met/ox}}{V_s^{met}} = J_O^{ox}u_A^{ox/met} - J_A^{ox} \tag{4.35}$$

The fluxes are defined positive in the same direction as z. The flux of A is thus negative and that of O is positive. It is seen that both equations give a positive interface velocity, which means that the oxide will grow in to the metal.

The flux balance equations can also be applied to the gas/oxide interface, now with β as the gas and α as the oxide. The gas usually does not contain any metal, thus $u_A^{gas/ox} = 0$ and $J_A^{gas} = 0$. As before, $u_O^{ox/gas} = 1$. Eq. 4.32 becomes:

$$\frac{v^{ox/gas}u_A^{ox/gas}}{V_s^{ox}} = J_A^{ox} \tag{4.36}$$

Since the flux of A is negative, the interface's velocity is negative. Thus, the oxide grows outward.

Chapter 5

In retrospect

Through the use of the Calphad methodology, this thesis heavily depends on reliable experimental work. It also happens so, that both the thermodynamic and diffusion parts involve systems that are subject to large differences in the available literature data, resulting in very different conclusions about important aspects of the respective case. Clearly, this demonstrates that it is very important, and often also very difficult, to measure exactly what is intended despite very carefully conducted experiments.

The challenge of the Al-Ni-Ru system was mainly to understand whether or not there is a miscibility gap in the ordered intermetallic B2 phase between NiAl and RuAl. That phase may be used as a bond coat, see fig. 1.1. From the literature, three different conclusions regarding the position and existence of the miscibility gap was found, and at a maximum only one of them can be correct. Supported by ab initio calculations it was concluded that, likely, there is no high temperature miscibility gap, although one is predicted below 280 K.

Diffusion in the almost stoichiometric oxides Cr_2O_3 and Fe_2O_3 also proves hard to measure reproducibly. One clear example is [17, 18], who measured the tracer diffusion coefficient in Fe_2O_3. They performed two seemingly identical experiments with material from the same specimen, but on two different days. The result was a 20 times difference in the measured tracer diffusion coefficient.

The differences are extremely large, for Cr up to about eight orders of magnitude, in the tracer diffusion data of Cr and O in Cr_2O_3. Of the oxides studied in this thesis, Cr_2O_3 is clearly the most difficult one to measure the intrinsic diffusion behavior in.

Keeping the contradictory data for Fe_2O_3 and Cr_2O_3 in mind it is interesting to

look at fig. 5 of paper IV, in which the tracer diffusion coefficient of Fe in Fe_3O_4 for some constant oxygen activities is calculated. It indicates that if the defect structure were not so well known, it would be very easy to draw conclusions based on some wrong assumptions. Knowing the defect structure for Fe_3O_4, it would not be so surprising to experimentally measure a diffusion coefficient that increases with decreasing temperature. In addition to the importance of producing very pure sample alloys, that could be another reason for the large differences we see for Fe_2O_3 and Cr_2O_3.

Chapter 6

Summary of appended papers

Paper I. Thermodynamic Assessment of the Ni-Ru system
In this report, a thermodynamic assessment of the binary system Ni-Ru was made. This system is of interest for calculations of thermodynamic properties of superalloys containing Ru. Superalloys are used in hot parts of gas turbine enginges for generation of electrical power or propulsion of aircraft.

The present author did all the work.

Paper II. Thermodynamic reassessment of the Ni-Ru system and assessment of the Al-Ni-Ru system at 1273-1523 K using *ab initio* calculations
In this report, thermodynamic assessments of the Ni-Ru and Al-Ni-Ru systems, with a combined Calphad and *ab initio* approach are presented. The systems are of interest for thermodynamic calculations of superalloys containing Ru. Superalloys are used in hot parts of gas turbine enginges for generation of electrical power or propulsion of aircraft. Attempts to perform diffusion simulations in the Ni-Ru system revealed unrealistic values of interaction parameters in the work of Paper I. Along with the assessment work of the Al-Ni-Ru system, the Ni-Ru system was reassessed with physically more sound parameters.

In the Al-Ni-Ru system, it is unclear whether or not there exists a miscibility gap in the BCC-B2 phase between the two B2 phases based on the binary intermetallic phases NiAl and RuAl. *Ab initio* calculations contributed to increased understanding of that uncertainty.

The present author did the thermodynamic assessments and wrote the thermodynamic assessment part of the paper.

Paper III. Modeling of diffusion in wustite and simulation of oxidation of iron at 600°C
In this report a diffusion model, optimization of mobilities in wustite, and simulation of diffusion of cations in the three iron oxides wustite, hematite and magnetite is presented. It is shown how rule of thumb values of the grain boundary mobilities can be used for taking into account grain boundary diffusion and retrieve satisfactory results.

The present author did the all the calculations and wrote the paper under supervision of the supervisor.

Paper IV. Modeling of iron diffusion in the iron oxides magnetite and hematite with variable stoichiometry
In this report a vacancy model of diffusion is applied to magnetite and hematite. Mathematical expressions for the iron flux in the lattice-fixed frame of reference, as a function of the defect structure, are presented. The model is validated against available experimental data, which gives excellent agreement for magnetite. For hematite, literature reports anomalous large activation energies and frequency factors. The scatter in reported values is also very large. For hematite a compromise solution is suggested.

The present author contributed to the model implementation, did all calculations and wrote parts of the paper.

Paper V. High temperature oxidation of chromium: kinetic modeling combined with microstructural investigation
This report is a combined experimental and theoretical work on high temperature oxidation of nominally pure Cr. Furnace exposures of Cr at 625°C and 700°C are performed, and the resulting specimen are investigated with respect to mass gain, morphology and microstrucre, using SEM and TEM.

Vacancy diffusion models for diffusion of O and Cr are presented, as well as an approach to take into account grain boundary diffusion. The models are validated against experimental data, which for chromia is very scattered. A compromise suggestion is presented, giving reasonable result.

The present author contributed to the model implementation, did all calculations and wrote parts of the paper.

Bibliography

[1] R.C. Reed, The Superalloys: Fundamentals and Applications, Cambridge University Press, 2006

[2] A.G. Evans, D.R. Clarke, C.G. Levi, J Eur Ceram Soc, 2008; 28: 1405-1419

[3] R. Vaßen, Thermal Barrier Coatings, In: R. Riedel, I-W Chen, editors. Ceramics Science and Technology Vol. 4: Wiley-VCH Verlag GmbH & Co. KGaA, 95-115

[4] S.R. Holdsworth, Creep-Fatigue in Steam Turbine Materials, In: D. Gandy, J. Shingledecker, R. Viswanathan, editors. Advances in Materials Technology for Fossil Power Plants: Proceedings of the Sixth International Conference (2010 Edition). Materials Park, OH, USA. ASM International; 2011

[5] T. Jonsson, B. Pujilaksono, H. Heidari, F. Liu, J-E. Svensson, M. Halvarsson L-G. Johansson, Corros Sci, 2013; 75; 326-336

[6] J.-O. Andersson, T. Helander, L. Höglund, P.F. Shi, B. Sundman, Calphad, 2002; 26: 273-312

[7] TC-Toolbox for MATLAB® Programmer's Guide, (Accessed 7 April 2014)

[8] Materials Genome Initiative for Global Competitiveness; http://www.whitehouse.gov/sites/default/files/microsites/ostp/materials_genome_initiative-final.pdf, (Accessed 31 August 2014)

[9] L. Kaufman, J. Agren, Scripta Mater, 2014; 70: 3-6

[10] P.J. Spencer, Calphad, 2008; 32(1): 1-8

[11] M. Hillert, J. Alloys Comp, 2001; 320: 161-176

[12] J.-O. Andersson and J. Ågren, J Appl Phys, 1992; 72(4): 1350-1355

[13] T. Helander, J. Ågren, Acta Mater, 1999; 47: 1141-1152

[14] C. Wagner, Z Phys Chem, 1933; B 21: 25-41

[15] C. Wagner, Prog Solid State Ch, 1975; 10(1): 3-16

[16] R.D. Shannon, Acta Cryst, 1976; A32: 751-767

[17] K. Hoshino, NL. Peterson, J Phys Solids, 1985; 46: 375

[18] K. Hoshino, NL. Peterson, J Phys Solids, 1985; 46: 1247

[19] NL. Peterson, WK. Chen, D. Wolf, J Phys Chem Solids, 1980; 41: 709

[20] I. Kaur, W. Gust, Fundamentals of grain and interphase boundary diffusion, Ziegler Press; 1989